https://doi.org/10.5194/gmd-2020-95
Preprint. Discussion started: 19 June 2020

Geoscientific Model Development Discussions

A fully coupled Arctic sea ice-ocean-atmosphere model (ArcIOAM v1.0) based on C-Coupler2: model description and preliminary results

Shihe Ren[1], Xi Liang[1], Qizhen Sun[1], Hao Yu[2], L. Bruno Tremblay[3], Xiaoping Mai[1], Fu Zhao[1], Ming Li[1], Na Liu[1], Zhikun Chen[1], Yunfei Zhang[1]

[1]Key Laboratory of Research on Marine Hazards Forecasting, National Marine Environmental Forecasting Center, Ministry of Natural Resources, Beijing, China
[2]Ministry of Education Key Laboratory for Earth System Modelling, Department of Earth System Science, Tsinghua University, Beijing, China
[3]Department of Atmospheric and Oceanic Sciences, McGill University, Montreal, Canada

Correspondence to: Xi Liang (liangx@nmefc.cn)

Abstract. The implementation of a new Arctic regional coupled sea ice-ocean-atmosphere model (ArcIOAM) and its preliminary results in the year of 2012 are presented in this paper. A newly developed coupler, C-Coupler2 (the Community Coupler 2), is used to couple the Arctic sea ice-oceanic configuration of the MITgcm (Massachusetts Institute of Technology general circulation model) with the Arctic atmospheric configuration of the Polar WRF (Weather Research and Forecasting) model. ArcIOAM is demonstrated with focus on seasonal simulation of the Arctic sea ice and ocean state in the year of 2012. The results obtained by ArcIOAM, along with the experiment of one-way coupling strategy, are compared with available observational data and reanalysis products. From the comparison, results obtained from two experiments both realistically capture the sea ice and oceanic variables in the Arctic region over a 1-year simulation period. The two-way coupled model has better performance in terms of sea ice extent, concentration, thickness and SST, especially in summer. This indicates that sea ice-ocean-atmosphere interaction takes a crucial role in controlling Arctic summertime sea ice distribution. The coupled model and documentation are available at https://doi.org/10.5281/zenodo.3742692 (last access: 9 June 2020), and the source code is maintained at https://github.com/cdmpbp123/Coupled_Atm_Ice_Oce (last access: 7 April 2020).

1 Introduction

It has been widely recognized that coupling between different earth system components (ocean, atmosphere, sea ice, and land) could provide improved forecasts of oceanic and atmospheric states on various timescales (Neelin et al., 1994). As an essential component in climate system, sea ice plays a crucial role in global energy and water budget, and has a substantial impact on local and remote atmospheric and oceanic circulations. In polar region, strong interactions between different interfaces disturb sea ice motion and affect sea ice growth-melt process (Jung et al., 2016). Due to the combined features of solid and fluid, sea ice thermodynamical and dynamical representations in coupled models can be complicated. In recent

https://doi.org/10.5194/gmd-2020-95
Preprint. Discussion started: 19 June 2020


Geoscientific Model Development Discussions

years, marine traffic through the Arctic are projected to become increasingly feasible as climate change continues, which has amplified the demand for reliable polar sea ice and marine environmental predictions from synoptic timescale to seasonal and interannual timescales.

In the past decades, a number of coupled models have been developed with various sea ice prediction capacities on various time scales (Pellerin et al., 2004;Williams et al., 2018;Chen et al., 2010;Skachko et al., 2019). Climate models, such as those involved in the Coupled Model Intercomparison Project Phase 5 (CMIP5), normally incorporate sea ice model in a relatively simple way, thus can be used to generate long-term sea ice outlook with low confidence on spatial distribution. Recently within the GODAE (Global Ocean Data Assimilation Experiment) Oceanview community, there is an increasing interest of using coupled global models to predict sea ice on shorter time scales (Brassington et al., 2015). In Canada, a coupled global forecasting system is now running operationally at the Canadian Centre for Meteorological and Environmental Prediction (Smith et al., 2018), providing global 10 days forecasts of ocean and sea ice states. The ocean-sea ice components of this system, namely the Global Ice-Ocean Prediction System (GIOPS, runs in real time since March 2014) (Smith et al., 2016), are based on the Nucleus for European Modelling of the Ocean (NEMO) and the Community Ice CodE (CICE) model. The GIOPS is coupled to an operational global deterministic medium-range weather forecasting system, namely the Global Deterministic Prediction System (GDPS) (Smith et al., 2014), which is based on the Global Environmental Multiscale (GEM) atmosphere model. In the United Kingdom, Hadley Centre Global Environment Model version 3 (HadGEM3) is under development and is planning to service in seasonal sea ice prediction (Williams et al., 2018). The HadGEM3 is constitute of the UK Met Office Unified Model (UKMO UM) atmosphere model (Walters et al., 2011), the Joint UK Land Environment Simulator land-surface model (Brown et al., 2012), the NEMO model and the CICE model. In the United States, a coupled global sea ice-ocean-wave-land-atmosphere prediction system providing operational daily predictions out to 10 days and weekly predictions out to 30 days is being developed by the US Navy (Brassington et al., 2015;Posey et al., 2015).

Although global coupled models are now being implemented with increased horizontal resolution, higher-resolution regional coupled models can provide an affordable way to study interactive ocean-atmosphere and sea ice-atmosphere feedback for polar weather and sea ice process, if properly forced by initial and boundary conditions. On the regional scale, there are also a few coupled sea ice-ocean-atmosphere model systems for the Arctic climate study and operational sea ice forecast. Schrum et al. (2003) introduced a coupled sea ice-ocean-atmosphere model for the North and Baltic Seas. In their work, the regional atmospheric model REgional MOdel (REMO) was coupled to the HAMburg Shelf Ocean Model (HAMSOM) with a sea ice module. Pellerin et al. (2004) demonstrated that significant sea ice forecasting improvements occurred when implemented the two-way coupling between the Gulf of St. Lawrence model with the GEM atmosphere model. Van Pham et al. (2014) compared basin-scale climate simulation in the regional coupled model COSMO-CLM-NEMO with that in the stand-alone COSMO-CLM model for the North and Baltic Seas, and found large improvement in the simulated atmospheric low boundary temperature. As part of the Canadian Operational Network of Coupled Environmental PredicTion Systems (CONCEPTS), a fully coupled sea ice-ocean-atmosphere forecasting system for the Gulf of St. Lawrence has been developed (Faucher et al., 2009) and running operationally at the Canadian Meteorological Centre since June 2011. The new

https://doi.org/10.5194/gmd-2020-95
Preprint. Discussion started: 19 June 2020


Geoscientific Model Development Discussions

model developing plan is to couple a high-resolution (1/12 degree) sea ice-ocean regional model which covering the North Atlantic and Arctic Ocean (Dupont et al., 2015) to the regional weather prediction system and wave prediction system of Environment Canada and provide short-term sea ice-ocean predictions to users.

This work is motivated by the need of a coupled Arctic sea ice-ocean-atmosphere model system for seasonal sea ice prediction in National Marine Environmental Forecasting Center of China. In coupled model systems, moisture, heat and momentum are often accomplished through the use of a separate coupling software like OASIS-MCT (Craig et al., 2017) or framework like the Earth System Model Framework (ESMF) (DeLuca et al., 2012) which links component models flexibly and controls the exchange and interpolation of coupling variables. The coupler, which can handle data interpolation and data transfer between different models and different grids, is the crucial part in the coupled systems. Using the ESMF and the National United Operational Prediction Capability (NUOPC), Sun et al. (2019) introduced a regional ocean-atmosphere coupled model covering the Red Sea based on the Massachusetts Institute of Technology general circulation model (MITgcm) (Marshall et al., 1997) and the Weather Research and Forecasting (WRF) model (Skamarock et al., 2008).

In our study, we use a newly developed efficient coupling framework, the Community Coupler 2 (C-Coupler 2) (Liu et al., 2018), to couple the Arctic sea ice-oceanic configuration of the MITgcm (Nguyen et al., 2011;Liang and Losch, 2018) with the Arctic atmospheric configuration of the Polar WRF model (Hines and Bromwich, 2008) model. By coupling the Polar WRF and the MITgcm for the first time in Arctic region, to this end, a series of specific procedures including data interpolation between different grids and relaxation algorithm in specific areas are developed. After implementing ArcIOAM, we run seasonal simulation of Arctic sea ice and ocean state in 2012. The simulated variables of the Arctic ocean and sea ice are examined and validated against available observational data and reanalysis products. To evaluate the role of sea ice-ocean-atmosphere interaction in Arctic sea ice seasonal cycle, we compare the simulation result of the two-way coupling experiment with that of the one-way coupling experiment in which the coupling variables are only transmitted from the Polar WRF to the MITgcm.

The paper is organized as follows. The description of the component models and coupling strategy are detailed in Section 2. Section 3 introduces the design of coupling experiments. Section 4 discusses the preliminary results in the validation test. The last section concludes the paper and presents an outlook for future work.

2 Model Description

2.1 The Oceanic and Sea Ice Component Model

The ocean and sea ice component of ArcIOAM is an Arctic configuration of the MITgcm (Nguyen et al., 2011;Liang and Losch, 2018;Liang et al., 2019). The model has an average horizontal resolution of 18 km and covers the whole Arctic Ocean with open boundaries close to 55 °N in both the Atlantic and Pacific sectors (Losch et al., 2010). The ocean model includes 420x384 horizontal grid points and 50 vertical model layers based on Arakawa C grid and Z coordinates. The ocean model uses curvilinear coordinates and the model grid is locally orthogonal. Vertical resolution of the ocean model layers

https://doi.org/10.5194/gmd-2020-95
Preprint. Discussion started: 19 June 2020


Geoscientific Model Development Discussions

increases from 10 m near the surface to 456 m near the bottom. The K-profile parameterization (KPP) (Large et al., 1994) is used as the vertical mixing scheme. Time step is 1200 seconds.

The sea ice model shares the same horizontal grid with the ocean model and divides each model grid into two parts: ice and open ocean. In the open ocean area, ocean-atmosphere heat and momentum fluxes are calculated following the standard bulk formula (Doney et al., 1998). In the ice-covered area, the ice surface and bottom heat and momentum fluxes are calculated according to viscous-plastic dynamics and zero-layer thermodynamics (Hibler, 1980;Semtner, 1976). The so-called zero-layer thermodynamic model assumes one-layer ice underneath one-layer snow and ice does not store heat, therefore tends to exaggerate the seasonal variability in ice thickness. Snow modifies ice surface albedo and conductivity. If enough snow accumulates on top of the ice, its weight submerges the ice and the snow is flooded.

2.2 The Atmospheric Component Model

The atmospheric component of ArcIOAM is based on the Arctic configuration of the Polar WRF (Bromwich et al., 2013;Hines and Bromwich, 2008) model, which is an optimized version of the WRF model (Skamarock et al., 2008) for use in polar region. The Polar WRF is developed and maintained by the Polar Meteorology Group at the Byrd Polar and Climate Research Center of the Ohio State University. In the Arctic configuration of the Polar WRF model, modifications for polar environments primarily encompass the land surface model and sea ice to adapt to the particular conditions in Arctic Regions. Two key modifications for the Polar WRF are optimization of surface energy balance and heat transfer for the Noah land surface model over sea ice and permanent ice surfaces, and a fix to allow specified sea ice quantities and the land mask associated with sea ice to update during a simulation. These modifications improve model performance over the pan-Arctic for short-term forecasts.

The Arctic configuration of the Polar WRF model has been tested and evaluated by a set of simulations over several key surface categories, including large permanent ice sheets with the Greenland/North Atlantic grid and Arctic land (Hines et al., 2011;Hines and Bromwich, 2008) and the production of the Arctic System Reanalysis (ASR) (Bromwich et al., 2010). In this study, the Polar WRF model covers the Arctic regions with a horizontal resolution of 27 km. The model has 306x306 horizontal grid points and 60 vertical layers. The prognostic equations in the Polar WRF model are solved with a time step of 120 seconds. The Polar WRF model employed physics options that included the Mellor Yamada-Janjic boundary layer scheme in conjunction with the Janjic-Eta Monin Obukhov surface layer scheme (Janjić, 2002), the WRF single-moment 6-class microphysics scheme for microphysics, the Grell-Devenyi scheme for clouds (Grell and Dévényi, 2002), and the new version of the rapid radiative transfer model for both shortwave and longwave radiation.

2.3 The Coupler Component Model

We use the C-Coupler 2 to couple the MITgcm and the Polar WRF model. The C-Coupler family was initiated from 2010 in China. The first version (C-Coupler1) includes features such as flexible coupling configuration and 3-D coupling capability (Liu et al., 2014). Two coupled models have been built using the C-Coupler1. The first is a coupled climate system model

https://doi.org/10.5194/gmd-2020-95
Preprint. Discussion started: 19 June 2020


Geoscientific Model Development Discussions

version FGOALS-gc at the Institute of Atmospheric Physics, Chinese Academy of Sciences. The FGOALS-gc can achieve exactly the same (bitwise identical) simulation results as same model components with different coupler the CPL6 (Liu et al., 2014). The second is a regional coupled model FIO-AOW (Zhao et al., 2017) which includes an atmosphere model WRF, an ocean model POM (Princeton Ocean Model) , and a wave model MASNUM (Yang et al., 2005).

The second version of the C-Coupler family, the C-Coupler 2 (Liu et al., 2018), is equipped with many advanced functions, including 1) a common, flexible, user-friendly coupling configuration interface, 2) the capability of coupling within one executable or the same subset of Message Passing Interface (MPI) processes, 3) flexible and automatic coupling procedure generation for any subset of component models, 4) dynamic 3-D coupling that enables convenient coupling of field on 3-D grids with time-evolving vertical coordinate values, 5) non-blocking data transfer, 6) facilitation for model nesting, 7) facilitation for increment coupling and 8) adaptive restart capability (Liu et al., 2018).

2.4 Coupling Strategy

The C-Coupler2 is employed as a library to achieve the two-way parallel coupling between the Polar WRF and the MITgcm (Figure 1). The coupling interval is set to 20 minutes. At each coupling time step, the MITgcm is executed when the Polar WRF model is completed and vice versa. During coupling execution, the MITgcm sends SST, sea ice concentration, sea ice thickness, snow depth and ice surface albedo to the coupler, and these coupling variables are used directly as the bottom boundary conditions in the Polar WRF model. The Polar WRF model sends the atmospheric bottom boundary variables to the coupler, including downward longwave radiation, downward shortwave radiation, 10-m wind speed, 2-m air temperature, 2-m air specific humidity, and precipitation. The MITgcm uses these atmospheric variables to compute the open ocean and ice surface heat, freshwater and momentum forcing.

Model domain of the MITgcm and the Polar WRF model are shown in Figure 2a. As the model domain and grid of the Polar WRF and the MITgcm are generally different, several important procedures have been carried out in conducting our coupled system:

1) The model domain of the Polar WRF is larger than that of the MITgcm, there is a non-overlapped area between the MITgcm domain and the Polar WRF domain. Besides, the MITgcm model only produces surface variables over ocean, and the Polar WRF model also needs bottom boundary conditions over land. Thus, the coupling variables received by the Polar WRF model need to be concatenated by value in the non-overlapped area and in the land area from an external forcing file, and value in the overlapped ocean area from the MITgcm model together. To diminish the abrupt value changes from two sources, a simple linear relax zone is designed near the open boundaries of the MITgcm model in both the Atlantic and Pacific sectors (Figure 2b). The coupling variables ($VAR_{recbyWRF}$) received by the Polar WRF model can be expressed as:

$$VAR_{recbyWRF} = (1-\alpha)VAR_{sedbyMIT} + \alpha VAR_{extern} \quad (1)$$

where α is relaxation coefficient, which is equal to 0 in the overlapped ocean area away from the MITgcm open boundaries, and equal to 1 in the land area and in the non-overlapped area away from the MITgcm open boundaries. While in the relax

https://doi.org/10.5194/gmd-2020-95
Preprint. Discussion started: 19 June 2020

Geoscientific Model Development Discussions

zone, α increases from 0 to 1 linearly from the overlapped side to the non-overlapped side. $VAR_{sedbyMIT}$ is the coupling variables which are send by the MITgcm model. VAR_{extern} is the bottom boundary variables of the Polar WRF model which are read from external forcing file.

2) The MITgcm model uses curvilinear grid whose horizontal resolution is variable. The Polar WRF model uses polar stereographic grid whose horizontal resolution is constant. Because the Polar WRF domain covers the MITgcm domain, the coupling interpolation from the Polar WRF grid to the MITgcm grid is straightforward, but the coupling interpolation from the MITgcm grid to the Polar WRF grid creates irregularities if the detailed geographic information of the MITgcm model grid is not specified. Meanwhile the MITgcm model is based on Arakawa C grid, geographic information of each grid cell is given at the center of the grid cell and at the four centers of the four boundaries of the grid cell. To correctly handle data interpolation between the different grids, the C-Coupler2 automatically calculates geographic information at the four corners of each grid cell (Figure 3) during the coupling initialization process. Take the left bottom corner (*v1*) of grid cell (i, j) as an example, the longitude (x_{v1}) and latitude (y_{v1}) are calculated as follows:

$$x_{v1} = \frac{x_{point(i-1,j)}+x_{point(i,j)}+x_{point(i-1,j-1)}+x_{point(i,j-1)}}{4} \quad (2)$$

$$y_{v1} = \frac{y_{point(i-1,j)}+y_{point(i,j)}+y_{point(i-1,j-1)}+y_{point(i,j-1)}}{4} \quad (3)$$

where the subscripts *point(i-1, j), point(i, j), point(i-1, j-1) and point(i, j-1)* denote the four centers of the four grid cells around the corner. In the following model execution or model restarting process, the C-Coupler2 uses the corner geographic information of the MITgcm grid to constrain interpolation domain from the MITgcm model to the Polar WRF model.

3 Numerical Experiments

The Arctic coupled model will be used to conduct seasonal sea ice prediction in our future plan. As a starting point, we need to evaluate the Arctic coupled model performance on seasonal timescale without any data assimilation. In this work, we perform the coupled model free simulations in the year of 2012 with special focuses on the summertime. With more open ocean area be exposed to atmosphere, we expect that sea ice-ocean-atmosphere interaction processes are relatively more intensified in the summertime than that in the wintertime. In the Arctic region, demands of seasonal prediction for sea ice and ocean are also strong in summertime when more commercial and scientific activities of Arctic shipping occur. Additionally, the year of 2012 is chosen because an unusually strong storm formed off the coast of Alaska on 5 August 2012, and tracked into the center of the Arctic Basin where it lingered for several days and generated stronger sea ice-ocean-atmosphere interaction (Simmonds and Rudeva, 2012). The main aim of this paper is to assess the sea ice and ocean simulation abilities of the coupled system. For this reason, less attention will be paid on the atmosphere simulation. Future work will emphasize atmospheric simulation and seasonal sea ice prediction skill with available observations be assimilated.

Two experiments using different coupling strategy are performed in this study. The first experiment which denoted by OCNCPL is a two-way coupled simulation that the MITgcm receives the coupled variables from the Polar WRF, and the

https://doi.org/10.5194/gmd-2020-95
Preprint. Discussion started: 19 June 2020


Geoscientific Model Development Discussions

Polar WRF also receives the coupled variables from the MITgcm. The second experiment which denoted by OCNDYN is a one-way coupled simulation that the MITgcm only receives the coupled variables from the Polar WRF, but without sending the coupled variables back to the Polar WRF. The model state deviation between the two runs represents the influences of sea ice-ocean-atmosphere interaction on the Arctic Ocean and sea ice.

The atmospheric specific initial and lateral boundary conditions, as well as bottom boundary conditions in the external forcing file, are derived from the 6-hourly National Centers for Environmental Prediction (NCEP) Climate Forecast System Reanalysis (CFSR) data (Saha et al., 2010). The oceanic monthly lateral boundary condition of the coupled model is derived from the Estimating the Circulation and Climate of the Ocean phase II (ECCO2): high-resolution global-ocean and sea ice data synthesis (Menemenlis et al., 2008), including potential temperature, salinity, current, and sea surface elevation. The discrepancy of atmosphere and ocean boundary condition is less of an issue since the ocean does not vary much on shorter time scale and the ice is far away from the lateral boundary. The ocean and sea ice initial condition on 1 January 2012 are derived from a stand-alone MITgcm simulation. The stand-alone MITgcm simulation was initialized from climatological temperature and salinity field derived from the World Ocean Atlas 2005 (WOA05) (Locarnini et al., 2006;Antonov et al., 2006) and forced by the 3-hourly Japanese 55-year Reanalysis data (JRA55) (Harada et al., 2016;Kobayashi et al., 2015) from 1979 to 2011 in our previous study (Liang and Losch, 2018). After 33-year integration, the ocean and sea ice initial condition on 1 January 2012 used in the coupled model are retrieved from a quasi-equilibrium ocean-sea ice evolution period. River runoff is based on the Arctic Runoff Data Base (Nguyen et al., 2011). The coupled model states are outputted on daily basis and used in our analysis.

4 Preliminary Results

4.1 Sea Ice Extent and Concentration

The lowest Arctic sea ice extent in the satellite-observed era occurred in the summer of 2012 (Francis, 2013). According to sea ice extent record derived from the Multisensor Analyzed Sea Ice Extent-North Hemisphere (MASIE-NH) (NSIDC, 2010), obtained from http://nsidc.org/data/masie/, in the year of 2012 Arctic sea ice extent grows to maximum value of 14.5 million km^2 in March and drops to minimum value of 3.5 million km^2 in September (Figure 4a). The MASIE-NH data is provided daily by the National Ice Center Interactive Multisensor Snow and Ice Mapping System with a spatial resolution of 4 km. Both the OCNCPL and OCNDYN run simulate lower sea ice extent than the observations by a bias of 1-2 million km^2 (Figure 4a) except the first half month of January. Because sea ice initial field on 1 January 2012 is derived from a stand-alone MITgcm simulation which is forced by the JRA55 data, the change of atmospheric forcing data from the JRA55 to the NCEP CFSR induces a model state adjustment period which lasts about half month. Comparing the sea ice extent evolution of the OCNCPL and OCNDYN run, it seems that sea ice-ocean-atmosphere interaction generates quite slight sea ice extent change, but based on our following analysis related to sea ice spatial distribution, sea ice-ocean-atmosphere interaction plays a decisive role in summertime sea ice spatial distribution.

https://doi.org/10.5194/gmd-2020-95
Preprint. Discussion started: 19 June 2020

Figure 4b shows the modeled and observed sea ice extent anomaly. After the model state adjustment period, both the amplitudes of sea ice extent seasonal cycle of the two runs are close to the observations. The sea ice extent bias between the model states and the observations likely arise from the sea ice model systematic bias which is induced by the choice of sea ice and snow albedo parameters in the two runs. Nguyen et al. (2011) pointed out that optimized parameters of sea ice and snow albedo depend on selected atmospheric forcing in the MITgcm. In the MITgcm sea ice model, the actual surface albedo changes with time and is a function of four foundational albedo parameters (dry ice, dry snow, wet ice, wet snow), as well as ice surface temperature and snow depth. The sea ice model systematic bias could be reduced by rationally amplifying albedo parameters or involving a sea ice data assimilation module (Liang et al., 2019) when conducting seasonal sea ice prediction system.

We compare the modeled sea ice concentration with the observations derived from the EUMETSAT Ocean and Sea Ice Satellite Application Facility (OSISAF) (Eastwood et al., 2011); obtained from http://osisaf.met.no/; product identifier: OSI-409. The observations are reprocessed daily sea ice concentration fields which are retrieved from the Scanning Multichannel Microwave Radiometer/Special Sensor Microwave Imager (SMMR/SSMI) data with a spatial resolution of 10 km. Figure 4c shows the root mean square error (RMSE) evolution of the modeled sea ice concentration with respect to the OSISAF data. The Arctic basin is almost fully covered by sea ice from January to May, thus the two experiments do not produce substantial sea ice concentration differences. Along with more open ocean are exposed to atmosphere, from June to September the sea ice concentration RMSE of the OCNCPL run is significantly lower than that of the OCNDYN run. This result indicates that sea ice-ocean-atmosphere interaction takes a crucial role in controlling Arctic summertime sea ice distribution.

To further clarify sea ice spatial distribution, we show the modeled and observed monthly mean sea ice concentration in July, August and September (Figure 5). In July, the modeled sea ice extent of the OCNCPL run is similar to that of the OCNDYN run, but the modeled sea ice concentration of the OCNCPL run is much lower than that of the OCNDYN run in thick multiyear ice zone near the Canadian Arctic Archipelago and in the southern Beaufort Sea (Figure 5a and Figure 5b). The satellite observations show that the OCNCPL run still overestimates sea ice concentration in the southern Beaufort Sea and the Laptev Sea (Figure 5c). In August, the modeled sea ice melts quickly in the Eurasian marginal seas in the two runs. Compared with the satellite observations (Figure 5f), the OCNDYN run overestimates sea ice concentration in the southern Beaufort Sea while underestimates sea ice concentration in the center Arctic basin (Figure 5e). The OCNCPL run simulates similar sea ice extent to the satellite observations but with lower concentration in the center Arctic basin (Figure 5d). In September, the modeled sea ice in the marginal sea ice zone melts out in the two runs. Although the two runs simulate almost same sea ice extent, due to rational representation of sea ice-ocean-atmosphere interaction in the OCNCPL run, the modeled sea ice distribution of the OCNCPL run is closer to the observations (Figure 5g and Figure 5i).

https://doi.org/10.5194/gmd-2020-95
Preprint. Discussion started: 19 June 2020


Geoscientific Model Development Discussions

255 **4.2 Sea Ice Volume and Thickness**

At current stage, satellite sea ice thickness data is not available in melting seasons from May to September. We compare the modeled sea ice volume with that from a widely used sea ice volume data source (Figure 6a), the Pan-Arctic Ice Ocean Modeling and Assimilation System (PIOMAS) developed at the Applied Physics Laboratory of the University of Washington (Zhang and Rothrock, 2003). The PIOMAS assimilates sea ice concentration data from the National Snow and
260 Ice Data Center (NSIDC) and SST data from NCEP/NCAR Reanalysis. Both the two runs produce less sea ice volume than the PIOMAS data almost in a whole year of 2012, partly resulting from that our model underestimates sea ice extent (Figure 4a) without assimilating any observation. However, it is notable that the sea ice volume evolution of the OCNCPL run is closer to the PIOMAS data at the end of 2012.

Satellite sea ice thickness observations are usually retrieved from either ice surface brightness temperature or radar altimetric
265 measurement of sea ice freeboard. We use three kinds of satellite sea ice thickness data to validate our model results (Figure 6b and Figure 6c). Daily sea ice thickness observations provided by the University of Hamburg are derived from the Soil Moisture Ocean Salinity (SMOS) brightness temperature combined with a sea ice thermodynamic model and a three-layer radiative transfer model (Kaleschke et al., 2012) obtained from http://icdc.cen.uni-hamburg.de/1/daten/cryosphere/l3c-smos-sit.html. Weekly sea ice thickness observations provided by the Alfred Wegener Institute, Helmholtz Centre for Polar and
270 Marine Research are derived from the European Space Agency satellite mission CryoSat-2 radar altimetric data (Ricker et al., 2014) obtained from http://data.meereisportal.de/data/cryosat2/version2.0/. The SMOS observations retrieved from satellite brightness temperature data have promised qualities in marginal sea ice zone where ice thickness is thinner than 1 m (Tian-Kunze et al., 2014) while the CryoSat-2 observations retrieved from radar altimetric data have higher accuracies in pack sea ice zone than in marginal sea ice zone (Laxon et al., 2013;Wingham et al., 2006). Taking the spatial complementarity of the
275 SMOS and CryoSat-2 data into consideration, Ricker et al. (2017) introduced a weekly sea ice thickness product covering the entire Arctic, the CS2SMOS sea ice thickness, which is generated by mathematically merging the SMOS sea ice thickness with the CryoSat-2 sea ice thickness (Ricker et al., 2017) obtained from https://data.meereisportal.de/data/cs2smos/version1.4/. The CS2SMOS data with observational uncertainty is also added in the comparison.

280 The weekly CryoSat-2 data is constitute of several banded sea ice thickness records which collected in one week when polar orbital satellite passes the Arctic region. The SMOS data used in this study are those in thin ice (< 1 m) region. Considering spatial coverage of the observations, we compare spatial-mean sea ice thickness evolution with the CS2SMOS data (Figure 6b). Comparing with the CS2SMOS data, both runs produce rational sea ice thickness evolution from January to April. However, large sea ice thickness errors between the model and the observations exist in October and November. We
285 attribute these large errors to the possibly observational uncertainties induced by radar altimetric measurement errors when ice surface starts to freeze up. The modeled sea ice in the OCNCPL run is thinner than that in the OCNDYN run, and the sea ice thickness deviations between the two runs amplify after the summer. Meanwhile the sea ice volume and thickness of the

https://doi.org/10.5194/gmd-2020-95
Preprint. Discussion started: 19 June 2020

OCNCPL run are closer to the PIOMAS data and the CS2SMOS observations at the end of 2012. We speculate that in the OCNCPL run sea ice-ocean-atmosphere interaction induces reasonable sea ice thickness distribution in the summer of 2012 which preconditions the sea ice thickness evolution in the following freezing season.

The sea ice thickness RMSEs of the two runs with respect to the three kinds of satellite sea ice thickness data are shown in Figure 6c. The sea ice thickness RMSE between the OCNCPL run and the SMOS data is smaller than that between the OCNDYN run and the SMOS data, indicating that sea ice-ocean-atmosphere interaction substantially improves the sea ice thickness simulation in the marginal sea ice zone in the OCNCPL run. The sea ice thickness RMSEs between model and the CryoSat-2 data are generally larger than those between model and the CS2SMOS data especially in October and November, which is partly due to the large uncertainty of radar altimetric measurement when ice surface starts to freeze up, and partly due to the low spatial coverage of the CryoSat-2 data.

Normally satellite sea ice thickness data has large uncertainty due to limitation of retrieval algorithm. In situ sea ice thickness observations with higher accuracy can provide a direct reference for the model. To further evaluate the modeled sea ice thickness, we compare the time evolution of modeled and observed sea ice thickness at three locations in the Beaufort Sea in 2012 (Figure 7). The observations are derived from moored upward-looking sonar (ULS) ice draft data from the Beaufort Gyre Exploration Project (BGEP) (Proshutinsky et al., 2005); obtained from http://www.whoi.edu/beaufortgyre/. The ULS samples the ice draft with a precision of 0.1 m (Melling and Riedel, 1995) , and the ice draft can be converted to ice thickness following the law of hydrostatic equilibrium (Nguyen et al., 2011). Generally speaking, at all three locations in the Beaufort Sea, when the modeled sea ice is thinner than 1 m, the sea ice thickness evolution improves in the OCNCPL run comparing with those in the OCNDYN run. This result further demonstrates that sea ice-ocean-atmosphere interaction plays an important role in marginal sea ice evolution.

Spatial distributions of monthly mean sea ice thickness in June, September, and December are shown in Figure 8. In June, almost the whole Arctic basin is still covered by thick ice, large sea ice thickness deviations between the two runs mainly appear around sea ice edge where sea ice-ocean-atmosphere interaction can impact significant influence on sea ice melting rate (Figure 8c). In September, accompanied by the change of sea ice concentration pattern when involving sea ice-ocean-atmosphere interaction, the modeled sea ice becomes thicker in the central Arctic while thinner in the area near the Greenland Island and in the southern Beaufort Sea (Figure 8f). As summertime sea ice thickness has strong effect on preconditioning the following wintertime sea ice thickness (Day et al., 2014), the modeled sea ice of the OCNCPL run is universally thinner than that of the OCNDYN run in December (Figure 8i).

4.3 Ocean Temperature and Current

Sea ice states are intimately linked to ocean states, both dynamically and thermodynamically. The modeled spatial distribution of sea ice concentration in the OCNCPL run exhibits great improvement comparing with the OCNDYN run. Since sea ice in marginal ice zone is strongly affected by SST through lateral heat transport, we suspect that sea ice-ocean-atmosphere interaction should impose positive influence on the modeled ocean temperature in the marginal sea ice zone.

https://doi.org/10.5194/gmd-2020-95
Preprint. Discussion started: 19 June 2020


Geoscientific Model Development Discussions

The modeled SST is validated against the Group for High-Resolution SST Multi-Product Ensemble (GMPE) data (obtained from http://marine.copernicus.eu/, product identifier: SST_GLO_SST_L4_NRT_OBSERVATIONS_010_005). The GMPE SST data provided by the UKMO is a reanalysis daily global SST product that computed as the median of a large number of SST products by various institutes around the world. Each product contributing to the GMPE product uses different observational data sets or different retrieval algorithms. As a median product of multiproduct ensemble, the GMPE SST data greatly reduces observational uncertainties. The SST RMSE of the two runs with respect to the GMPE data from July to September are shown in Figure 9. We do not show the time evolution of the SST RMSE in whole year because the two timeseries do not obviously diverge in the other months. In general, the SST RMSE of the OCNCPL run is smaller than that of the OCNDYN run in the summer of 2012, which means the SST simulation also improves when sea ice-ocean-atmosphere interaction is allowed in the model. Spatial patterns of modeled and observed SST in July, August and September are shown in Figure 10. The GMPE SST data is available in ice-free areas (Figure 10a, Figure 10e and Figure 10i). Comparing with the OCNDYN run, in July and August the modeled ocean surface of the OCNCPL run warms in Fram Strait, the Barents Sea, the Kara Sea and the Bering Strait while colds in the Baffin Bay, the Greenland Sea and the Laptev Sea (Figure 10d andFigure 10h). In September strong warming in the OCNCPL run appears in the southern Beaufort Sea (Figure 10l). These SST modifications induced by sea ice-ocean-atmosphere interaction not only lead to the reduction of the modeled ocean surface temperature bias, but also help to maintain a more rational sea ice spatial pattern.

Ocean current observations in the Arctic Ocean are quite sparse, we evaluate the modeled ocean velocity and temperature with climatological observation generated from the 1998-2003 mooring data in Fram Strait. Under the framework of the European Union projects Variability of Exchanges In the Northern Seas (VEINS) and Arctic Subarctic Ocean Fluxes - North (ASOF-N), a series of moorings in Fram Strait had been deployed to record ocean properties since September 1997 to 2004 (obtained from https://www.whoi.edu/page.do?pid=30914). The observation covers water column from 10 m above the seabed to about 50 m below the surface. Although the observations were conducted at least one decade earlier than 2012, we believe that the comparison between the modeled and observed monthly mean value would likely still make sense since the phase of the Atlantic Multidecadal Oscillation does not reverse between 1995 and 2012. The modeled and observed northward cross-section velocity and temperature averaged between 5°E and 8°40'E at 78°50'N are listed in Table 1. Basically, the observations show that the northward velocity of the West Spitsbergen Current (WSC) increases from July to September, and the mean temperature of the section of 78°50'N also increases from July to December. It is notable that the modeled velocity and temperature of the OCNCPL run in Fram Strait are closer to the observations comparing with those of the OCNDYN run, although there are still large biases of the modeled velocity between the OCNCPL run and the observations. Vertical temperature distribution in the section averaged between July and September shows that sea ice-ocean-atmosphere interaction induces warming of the WSC until 700 m depth accompanied with strong cooling beside the WSC (Figure 11c). The cross-section velocity deviation between the OCNCPL and OCNDYN run is characterized by enhanced northward velocity over the whole water column around 0 °E and east of 6 °E, while reduced northward velocity between them (Figure 11f).

https://doi.org/10.5194/gmd-2020-95
Preprint. Discussion started: 19 June 2020

355

5 Conclusion and Discussion

This paper describes the implementation of an Arctic regional sea ice-ocean-atmosphere coupled model (ArcIOAM). To connect the component models, a newly developed coupler, C-Coupler2 is implemented to couple the Arctic sea ice-oceanic configuration of the MITgcm model with the Arctic atmospheric configuration of the Polar WRF model. By coupling the Polar WRF and the MITgcm for the first time in Arctic region, a series of specific setup including data interpolation between different grids and relaxation algorithm in specific areas are designed.

After implementing the new coupled model of ArcIOAM, we demonstrate it on seasonal simulation of the Arctic sea ice and ocean state in 2012. Results from the two-way coupled simulation (OCNCPL) and the one-way coupled simulation (OCNDYN) are compared to a wide variety of available observational and reanalysis products. The model state deviation between two experiments represents the influences of sea ice-ocean-atmosphere interaction on the Arctic Ocean and sea ice. From the comparison, results obtained from two experiments both realistically capture the sea ice and oceanic variables in the Arctic region over a 1-year simulation period. The two-way coupled experiment gives equal or better results compared with the one-way coupled experiment.

Both the amplitudes of sea ice extent seasonal cycle of the two runs are close to the observations. The spatial distribution of sea ice concentration in the OCNCPL run is similar to that in the OCNDYN run from January to May. From June to September the sea ice concentration RMSE of the OCNCPL run with respect to the observations is significantly lower than that of the OCNDYN run, indicating that sea ice-ocean-atmosphere interaction takes a crucial role in controlling Arctic summertime sea ice distribution. The sea ice thickness RMSE of the OCNCPL run with respect to the SMOS data in thin ice areas is smaller than that of the OCNDYN run. Meanwhile, the evolution of the modeled and observed sea ice thickness at three locations in the Beaufort Sea show that the modeled sea ice thickness evolution improves in the OCNCPL run when the ice is thinner than 1m. This result means that sea ice-ocean-atmosphere interaction is very likely to improve the sea ice thickness simulation in the marginal sea ice zone when considering feedback of ocean to atmosphere. Based on comparison with a series of mooring data in Fram Strait, the modeled velocity and temperature in the OCNCPL run are closer to the observations than those in the OCNDYN run, although large biases of the modeled velocity still exist. Comparing with the satellite data, the SST obtained in the OCNCPL run is also better than that in the OCNDYN run in summer 2012. Due to strong sea ice-ocean-atmosphere interaction in summertime, the two-way coupling strategy.not only improves the sea ice simulation, but also benefit the modeled ocean states.

It is noticed that the simulation presented in this paper only covers one year, more seasonal scale simulations in different years should be carried out to further assess the coupled model. However, given the encouraging results in 2012, this new developed Arctic regional coupled model exhibits its potential capacity of seasonal sea ice prediction and provides a reliable basis for investigating both thermodynamic and dynamic process and forecasting applications in the Arctic sea ice scope.

https://doi.org/10.5194/gmd-2020-95
Preprint. Discussion started: 19 June 2020


Geoscientific Model Development Discussions

Meanwhile, bias in the modeled sea ice extent and summertime sea ice thickness still exist, although satellite sea thickness data normally has large uncertainty in summertime, which partly contributes to the large sea ice thickness bias in October-November between the model and CS2SMOS data (Figure 6b), the foundational sea ice albedo parameters in our current model configuration seem to be underestimated, which allows more heat into the ice and causes thinner sea ice thickness, as well as lower sea ice extent. The choice of sea ice albedo parameters also contributes to the large sea ice thickness bias in October-November between the model and CS2SMOS data. On the way to operational seasonal sea ice prediction, the model physics and model uncertainty representation in the coupled model can be enhanced using advanced techniques, such as stochastic physics parameterizations and ensemble approaches. The regional coupled forecasting system also can be improved by involving data assimilation capabilities for initializing the forecasts. Future work will involve exploring these and other aspects for a regional coupled modeling system suited for forecasting and process understanding.

Code and data availability. The latest version and future updates of the source code, user guide, and examples can be downloaded from https://github.com/cdmpbp123/Coupled_Atm_Ice_Oce (last access: 7 April 2020). The current version of this coupled model (ArcIOAM v1.0) used to produce the results in this paper can be accessed via https://doi.org/10.5281/zenodo.3742692.

Author contribution. SR and HY worked on the coding tasks for coupling the Polar WRF with the MITgcm using C-Coupler2. SR and XL designed and performed the simulations for the numerical experiments. SR, HY and XM worked on the technical details for debugging the model and wrote the code documentation. XL worked on the MITgcm model setup and performed sea ice analysis and validation. QS worked on the Polar WRF model setup. All authors contributed to the writing of the final article.

Competing interests. The authors declare that they have no conflict of interest.

Acknowledgments. This work is supported by the National Key R&D Program of China (2016YFC1402700, 2018YFC1407200) and the National Natural Science Foundation of China (41806003). The authors thank the University of Hamburg for providing the SMOS sea ice thickness data, the Alfred-Wegener-Institut, Helmholtz Zentrum für Polar- und Meeresforschung for providing the CryoSat-2, CS2SMOS sea ice thickness data and Fram Strait mooring data, the Norwegian Meteorological Institute for the OSISAF sea ice concentration data, the University of Washington for providing the PIOMAS sea ice volume data, the National Snow and Ice Data Center for providing the MASIE-NH data

https://doi.org/10.5194/gmd-2020-95
Preprint. Discussion started: 19 June 2020

(http://nsidc.org/data/masie/), the Woods Hole Oceanographic Institution for providing the BGEP ULS data (http://www.whoi.edu/beaufortgyre), and the Copernicus Marine Environment Monitoring Service for providing the GMPE SST data (http://marine.copernicus.eu/).

425

References

Antonov, J. I., Locarnini, R., Boyer, T., Mishonov, A., Garcia, H., and Levitus, S.: World Ocean Atlas 2005 Volume 2: Salinity, NOAA Atlas NESDIS, 62, 2006.

Brassington, G. B., Martin, M. J., Tolman, H. L., Akella, S., Balmeseda, M., Chambers, C. R. S., Chassignet, E., Cummings,
430 J. A., Drillet, Y., Jansen, P. A. E. M., Laloyaux, P., Lea, D., Mehra, A., Mirouze, I., Ritchie, H., Samson, G., Sandery, P. A., Smith, G. C., Suarez, M., and Todling, R.: Progress and challenges in short- to medium-range coupled prediction, Journal of Operational Oceanography, 8, s239-s258, 10.1080/1755876X.2015.1049875, 2015.

Bromwich, D., Kuo, Y.-H., Serreze, M., Walsh, J., Bai, L.-S., Barlage, M., Hines, K., and Slater, A.: Arctic System Reanalysis: Call for Community Involvement, Eos, Transactions American Geophysical Union, 91, 13-14,
435 10.1029/2010EO020001, 2010.

Bromwich, D. H., Otieno, F. O., Hines, K. M., Manning, K. W., and Shilo, E.: Comprehensive evaluation of polar weather research and forecasting model performance in the Antarctic, Journal of Geophysical Research: Atmospheres, 118, 274-292, 10.1029/2012JD018139, 2013.

Brown, A., Milton, S., Cullen, M., Golding, B., Mitchell, J., and Shelly, A.: Unified Modeling and Prediction of Weather and
440 Climate: A 25-Year Journey, Bulletin of the American Meteorological Society, 93, 1865-1877, 10.1175/BAMS-D-12-00018.1, 2012.

Chen, S., Campbell, T. J., Jin, H., Gaberšek, S., Hodur, R. M., and Martin, P.: Effect of Two-Way Air–Sea Coupling in High and Low Wind Speed Regimes, Monthly Weather Review, 138, 3579-3602, 10.1175/2009mwr3119.1, 2010.

Craig, A., Valcke, S., and Coquart, L.: Development and performance of a new version of the OASIS coupler, OASIS3-
445 MCT_3.0, Geosci. Model Dev., 10, 3297-3308, 10.5194/gmd-10-3297-2017, 2017.

DeLuca, C., Theurich, G., and Balaji, V.: The Earth System Modeling Framework, in: Earth System Modelling - Volume 3: Coupling Software and Strategies, edited by: Valcke, S., Redler, R., and Budich, R., Springer Berlin Heidelberg, Berlin, Heidelberg, 43-54, 2012.

Doney, S. C., Large, W. G., and Bryan, F. O.: Surface Ocean Fluxes and Water-Mass Transformation Rates in the Coupled
450 NCAR Climate System Model, Journal of Climate, 11, 1420-1441, 10.1175/1520-0442(1998)011<1420:sofawm>2.0.co;2, 1998.

https://doi.org/10.5194/gmd-2020-95
Preprint. Discussion started: 19 June 2020

Dupont, F., Higginson, S., Bourdallé-Badie, R., Lu, Y., Roy, F., Smith, G. C., Lemieux, J. F., Garric, G., and Davidson, F.: A high-resolution ocean and sea-ice modelling system for the Arctic and North Atlantic oceans, Geosci. Model Dev., 8, 1577-1594, 10.5194/gmd-8-1577-2015, 2015.

Eastwood, S., Larsen, K. R., Lavergne, T., Nielsen, E., and Tonboe, R.: Global sea ice concentration reprocessing Product User Manual, EUMETSAT OSISAF, 2011.

Faucher, M., Roy, F., Desjardins, S., Fogarty, C., Pellerin, P., Ritchie, H., and Denis, B.: Operational coupled atmosphere - ocean - ice forecast system for the Gulf of St. Lawrence, Canada, 9th EMS Annual Meeting, 2009,

Francis, J. A.: The where and when of wetter and drier: disappearing Arctic sea ice plays a role, Environmental Research Letters, 8, 041002, 10.1088/1748-9326/8/4/041002, 2013.

Grell, G. A., and Dévényi, D.: A generalized approach to parameterizing convection combining ensemble and data assimilation techniques, Geophysical Research Letters, 29, 38-31-38-34, 10.1029/2002gl015311, 2002.

Harada, Y., Kamahori, H., Kobayashi, C., Endo, H., Kobayashi, S., Ota, Y., Onoda, H., Onogi, K., Miyaoka, K., and Takahashi, K.: The JRA-55 Reanalysis: Representation of Atmospheric Circulation and Climate Variability, Journal of the Meteorological Society of Japan. Ser. II, 94, 269-302, 10.2151/jmsj.2016-015, 2016.

Hibler, W. D.: Modeling a Variable Thickness Sea Ice Cover, Monthly Weather Review, 108, 1943-1973, 10.1175/1520-0493(1980)108<1943:MAVTSI>2.0.CO;2, 1980.

Hines, K. M., and Bromwich, D. H.: Development and Testing of Polar Weather Research and Forecasting (WRF) Model. Part I: Greenland Ice Sheet Meteorology, Monthly Weather Review, 136, 1971-1989, 10.1175/2007mwr2112.1, 2008.

Hines, K. M., Bromwich, D. H., Bai, L.-S., Barlage, M., and Slater, A. G.: Development and Testing of Polar WRF. Part III: Arctic Land, Journal of Climate, 24, 26-48, 10.1175/2010JCLI3460.1, 2011.

Janjić, Z.: Nonsingular Implementation of the Mellor-Yamada Level 2.5 Scheme in the NCEP Meso model (NCEP Office Note No. 437), NCEP, Camp Springs, Md, 2002.

Jung, T., Gordon, N. D., Bauer, P., Bromwich, D. H., Chevallier, M., Day, J. J., Dawson, J., Doblas-Reyes, F., Fairall, C., Goessling, H. F., Holland, M., Inoue, J., Iversen, T., Klebe, S., Lemke, P., Losch, M., Makshtas, A., Mills, B., Nurmi, P., Perovich, D., Reid, P., Renfrew, I. A., Smith, G., Svensson, G., Tolstykh, M., and Yang, Q.: Advancing Polar Prediction Capabilities on Daily to Seasonal Time Scales, Bulletin of the American Meteorological Society, 97, 1631-1647, 10.1175/bams-d-14-00246.1, 2016.

Kaleschke, L., Tian-Kunze, X., Maaß, N., Mäkynen, M., and Drusch, M.: Sea ice thickness retrieval from SMOS brightness temperatures during the Arctic freeze-up period, Geophysical Research Letters, 39, 10.1029/2012GL050916, 2012.

Kobayashi, S., Ota, Y., Harada, Y., Ebita, A., Moriya, M., Onoda, H., Onogi, K., Kamahori, H., Kobayashi, C., Endo, H., Miyaoka, K., and Takahashi, K.: The JRA-55 Reanalysis: General Specifications and Basic Characteristics, Journal of the Meteorological Society of Japan. Ser. II, 93, 5-48, 10.2151/jmsj.2015-001, 2015.

Large, W. G., Mcwilliams, J. C., and Doney, S. C.: Oceanic vertical mixing: A review and a model with a nonlocal boundary layer parameterization, Reviews of Geophysics, 32, 363-403, 1994.

https://doi.org/10.5194/gmd-2020-95
Preprint. Discussion started: 19 June 2020

Laxon, S. W., Giles, K. A., Ridout, A. L., Wingham, D. J., Willatt, R., Cullen, R., Kwok, R., Schweiger, A., Zhang, J., Haas, C., Hendricks, S., Krishfield, R., Kurtz, N., Farrell, S., and Davidson, M.: CryoSat-2 estimates of Arctic sea ice thickness and volume, Geophysical Research Letters, 40, 732-737, 10.1002/grl.50193, 2013.

Liang, X., and Losch, M.: On the Effects of Increased Vertical Mixing on the Arctic Ocean and Sea Ice, Journal of Geophysical Research: Oceans, 123, 9266-9282, 10.1029/2018jc014303, 2018.

Liang, X., Losch, M., Nerger, L., Mu, L., Yang, Q., and Liu, C.: Using Sea Surface Temperature Observations to Constrain Upper Ocean Properties in an Arctic Sea Ice-Ocean Data Assimilation System, Journal of Geophysical Research: Oceans, 124, 4727-4743, 10.1029/2019jc015073, 2019.

Liu, L., Yang, G., Wang, B., Zhang, C., Li, R., Zhang, Z., Ji, Y., and Wang, L.: C-Coupler1: a Chinese community coupler for Earth system modeling, Geosci. Model Dev., 7, 2281-2302, 10.5194/gmd-7-2281-2014, 2014.

Liu, L., Zhang, C., Li, R., Wang, B., and Yang, G.: C-Coupler2: a flexible and user-friendly community coupler for model coupling and nesting, Geosci. Model Dev., 11, 3557-3586, 10.5194/gmd-11-3557-2018, 2018.

Locarnini, R. A., Mishonov, A., Antonov, J., Boyer, T., Garcia, H., and Levitus, S.: World Ocean Atlas 2005 Volume 1: Temperature NOAA Atlas NESDIS, 61, 2006.

Losch, M., Menemenlis, D., Campin, J.-M., Heimbach, P., and Hill, C.: On the formulation of sea-ice models. Part 1: Effects of different solver implementations and parameterizations, Ocean Modelling, 33, 129-144, https://doi.org/10.1016/j.ocemod.2009.12.008, 2010.

Marshall, J., Hill, C., Perelman, L., and Adcroft, A.: Hydrostatic, quasi-hydrostatic, and nonhydrostatic ocean modeling, Journal of Geophysical Research: Oceans, 102, 5733-5752, 10.1029/96jc02776, 1997.

Melling, H., and Riedel, D. A.: The underside topography of sea ice over the continental shelf of the Beaufort Sea in the winter of 1990, Journal of Geophysical Research: Oceans, 100, 13641-13653, 10.1029/95JC00309, 1995.

Menemenlis, D., J. M. Campin, P. Heimbach, C. Hill, T. Lee, A. Nguyen, M. Schodlok, and Zhang, H.: ECCO2: High resolution global ocean and sea ice data synthesis, Mercator Ocean Q. Newsl., 31, 13-21, 2008.

Neelin, J. D., Latif, M., and Jin, F.: Dynamics of Coupled Ocean-Atmosphere Models: The Tropical Problem, Annual Review of Fluid Mechanics, 26, 617-659, 10.1146/annurev.fl.26.010194.003153, 1994.

Nguyen, A. T., Menemenlis, D., and Kwok, R.: Arctic ice-ocean simulation with optimized model parameters: Approach and assessment, Journal of Geophysical Research: Oceans, 116, 10.1029/2010JC006573, 2011.

Pellerin, P., Ritchie, H., Saucier, F. J., Roy, F., Desjardins, S., Valin, M., and Lee, V.: Impact of a Two-Way Coupling between an Atmospheric and an Ocean-Ice Model over the Gulf of St. Lawrence, Monthly Weather Review, 132, 1379-1398, 10.1175/1520-0493(2004)132<1379:ioatcb>2.0.co;2, 2004.

Posey, P. G., Metzger, E. J., Wallcraft, A. J., Hebert, D. A., Allard, R. A., Smedstad, O. M., Phelps, M. W., Fetterer, F., Stewart, J. S., Meier, W. N., and Helfrich, S. R.: Improving Arctic sea ice edge forecasts by assimilating high horizontal resolution sea ice concentration data into the US Navy's ice forecast systems, The Cryosphere, 9, 1735-1745, 10.5194/tc-9-1735-2015, 2015.

https://doi.org/10.5194/gmd-2020-95
Preprint. Discussion started: 19 June 2020

Proshutinsky, A., Yang, J., Krishfield, R., Gerdes, R., Karcher, M., Kauker, F., Koeberle, C., Hakkinen, S., Hibler, W., Holland, D., Maqueda, M., Holloway, G., Hunke, E., Maslowski, W., Steele, M., and Zhang, J.: Arctic ocean study: Synthesis of model results and observations, Eos, Transactions American Geophysical Union, 86, 368-371, 10.1029/2005EO400003, 2005.

Ricker, R., Hendricks, S., Helm, V., Skourup, H., and Davidson, M.: Sensitivity of CryoSat-2 Arctic sea-ice freeboard and thickness on radar-waveform interpretation, The Cryosphere, 8, 1607-1622, 10.5194/tc-8-1607-2014, 2014.

Ricker, R., Hendricks, S., Kaleschke, L., Tian-Kunze, X., King, J., and Haas, C.: A weekly Arctic sea-ice thickness data record from merged CryoSat-2 and SMOS satellite data, The Cryosphere, 11, 1607-1623, 10.5194/tc-11-1607-2017, 2017.

Saha, S., Moorthi, S., Pan, H.-L., Wu, X., Wang, J., Nadiga, S., Tripp, P., Kistler, R., Woollen, J., Behringer, D., Liu, H., Stokes, D., Grumbine, R., Gayno, G., Wang, J., Hou, Y.-T., Chuang, H.-y., Juang, H.-M. H., Sela, J., Iredell, M., Treadon, R., Kleist, D., Delst, P. V., Keyser, D., Derber, J., Ek, M., Meng, J., Wei, H., Yang, R., Lord, S., Dool, H. v. d., Kumar, A., Wang, W., Long, C., Chelliah, M., Xue, Y., Huang, B., Schemm, J.-K., Ebisuzaki, W., Lin, R., Xie, P., Chen, M., Zhou, S., Higgins, W., Zou, C.-Z., Liu, Q., Chen, Y., Han, Y., Cucurull, L., Reynolds, R. W., Rutledge, G., and Goldberg, M.: The NCEP Climate Forecast System Reanalysis, Bulletin of the American Meteorological Society, 91, 1015-1058, 10.1175/2010bams3001.1, 2010.

Schrum, C., Hübner, U., Jacob, D., and Podzun, R.: A coupled atmosphere/ice/ocean model for the North Sea and the Baltic Sea, Climate Dynamics, 21, 131-151, 10.1007/s00382-003-0322-8, 2003.

Semtner, A. J.: A Model for the Thermodynamic Growth of Sea Ice in Numerical Investigations of Climate, Journal of Physical Oceanography, 6, 379-389, 10.1175/1520-0485(1976)006<0379:amfttg>2.0.co;2, 1976.

Simmonds, I., and Rudeva, I.: The great Arctic cyclone of August 2012, Geophysical Research Letters, 39, 10.1029/2012gl054259, 2012.

Skachko, S., Buehner, M., Laroche, S., Lapalme, E., Smith, G., Roy, F., Surcel-Colan, D., Bélanger, J. M., and Garand, L.: Weakly coupled atmosphere–ocean data assimilation in the Canadian global prediction system (v1), Geosci. Model Dev., 12, 5097-5112, 10.5194/gmd-12-5097-2019, 2019.

Skamarock, W. C., Klemp, J. B., Dudhia, J., Gill, D. O., Barker, D., and Duda, M. G.: A Description of the Advanced Research WRF Version 3 (No. NCAR/TN-475+STR), University Corporation for Atmospheric Research, 2008.

Smith, G. C., Roy, F., Mann, P., Dupont, F., Brasnett, B., Lemieux, J.-F., Laroche, S., and Bélair, S.: A new atmospheric dataset for forcing ice–ocean models: Evaluation of reforecasts using the Canadian global deterministic prediction system, Quarterly Journal of the Royal Meteorological Society, 140, 881-894, 10.1002/qj.2194, 2014.

Smith, G. C., Roy, F., Reszka, M., Surcel Colan, D., He, Z., Deacu, D., Belanger, J.-M., Skachko, S., Liu, Y., Dupont, F., Lemieux, J.-F., Beaudoin, C., Tranchant, B., Drévillon, M., Garric, G., Testut, C.-E., Lellouche, J.-M., Pellerin, P., Ritchie, H., Lu, Y., Davidson, F., Buehner, M., Caya, A., and Lajoie, M.: Sea ice forecast verification in the Canadian Global Ice Ocean Prediction System, Quarterly Journal of the Royal Meteorological Society, 142, 659-671, 10.1002/qj.2555, 2016.

https://doi.org/10.5194/gmd-2020-95
Preprint. Discussion started: 19 June 2020

Smith, G. C., Bélanger, J.-M., Roy, F., Pellerin, P., Ritchie, H., Onu, K., Roch, M., Zadra, A., Colan, D. S., Winter, B., Fontecilla, J.-S., and Deacu, D.: Impact of Coupling with an Ice–Ocean Model on Global Medium-Range NWP Forecast Skill, Monthly Weather Review, 146, 1157-1180, 10.1175/MWR-D-17-0157.1, 2018.

Sun, R., Subramanian, A. C., Miller, A. J., Mazloff, M. R., Hoteit, I., and Cornuelle, B. D.: SKRIPS v1.0: a regional coupled ocean–atmosphere modeling framework (MITgcm–WRF) using ESMF/NUOPC, description and preliminary results for the Red Sea, Geosci. Model Dev., 12, 4221-4244, 10.5194/gmd-12-4221-2019, 2019.

Tian-Kunze, X., Kaleschke, L., Maaß, N., Mäkynen, M., Serra, N., Drusch, M., and Krumpen, T.: SMOS-derived thin sea ice thickness: algorithm baseline, product specifications and initial verification, The Cryosphere, 8, 997-1018, 10.5194/tc-8-997-2014, 2014.

Van Pham, T., Brauch, J., Dieterich, C., Frueh, B., and Ahrens, B.: New coupled atmosphere-ocean-ice system COSMO-CLM/NEMO: assessing air temperature sensitivity over the North and Baltic Seas, Oceanologia, 56, 167-189, https://doi.org/10.5697/oc.56-2.167, 2014.

Walters, D. N., Best, M. J., Bushell, A. C., Copsey, D., Edwards, J. M., Falloon, P. D., Harris, C. M., Lock, A. P., Manners, J. C., Morcrette, C. J., Roberts, M. J., Stratton, R. A., Webster, S., Wilkinson, J. M., Willett, M. R., Boutle, I. A., Earnshaw, P. D., Hill, P. G., MacLachlan, C., Martin, G. M., Moufouma-Okia, W., Palmer, M. D., Petch, J. C., Rooney, G. G., Scaife, A. A., and Williams, K. D.: The Met Office Unified Model Global Atmosphere 3.0/3.1 and JULES Global Land 3.0/3.1 configurations, Geosci. Model Dev., 4, 919-941, 10.5194/gmd-4-919-2011, 2011.

Williams, K. D., Copsey, D., Blockley, E. W., Bodas-Salcedo, A., Calvert, D., Comer, R., Davis, P., Graham, T., Hewitt, H. T., Hill, R., Hyder, P., Ineson, S., Johns, T. C., Keen, A. B., Lee, R. W., Megann, A., Milton, S. F., Rae, J. G. L., Roberts, M. J., Scaife, A. A., Schiemann, R., Storkey, D., Thorpe, L., Watterson, I. G., Walters, D. N., West, A., Wood, R. A., Woollings, T., and Xavier, P. K.: The Met Office Global Coupled Model 3.0 and 3.1 (GC3.0 and GC3.1) Configurations, Journal of Advances in Modeling Earth Systems, 10, 357-380, 10.1002/2017ms001115, 2018.

Wingham, D. J., Francis, C. R., Baker, S., Bouzinac, C., Brockley, D., Cullen, R., de Chateau-Thierry, P., Laxon, S. W., Mallow, U., Mavrocordatos, C., Phalippou, L., Ratier, G., Rey, L., Rostan, F., Viau, P., and Wallis, D. W.: CryoSat: A mission to determine the fluctuations in Earth's land and marine ice fields, Advances in Space Research, 37, 841-871, https://doi.org/10.1016/j.asr.2005.07.027, 2006.

Yang, Y., Qiao, F., Zhao, W., Y., T., and Yuan, Y.: MASNUM ocean wave numerical model in spherical coordinates and its application, Acta Oceanol. Sin., 27, 1-7, 2005.

Zhang, J., and Rothrock, D. A.: Modeling Global Sea Ice with a Thickness and Enthalpy Distribution Model in Generalized Curvilinear Coordinates, Monthly Weather Review, 131, 845-861, 10.1175/1520-0493(2003)131<0845:mgsiwa>2.0.co;2, 2003.

Zhao, B., Qiao, F., Cavaleri, L., Wang, G., Bertotti, L., and Liu, L.: Sensitivity of typhoon modeling to surface waves and rainfall, Journal of Geophysical Research: Oceans, 122, 1702-1723, 10.1002/2016jc012262, 2017.

https://doi.org/10.5194/gmd-2020-95
Preprint. Discussion started: 19 June 2020

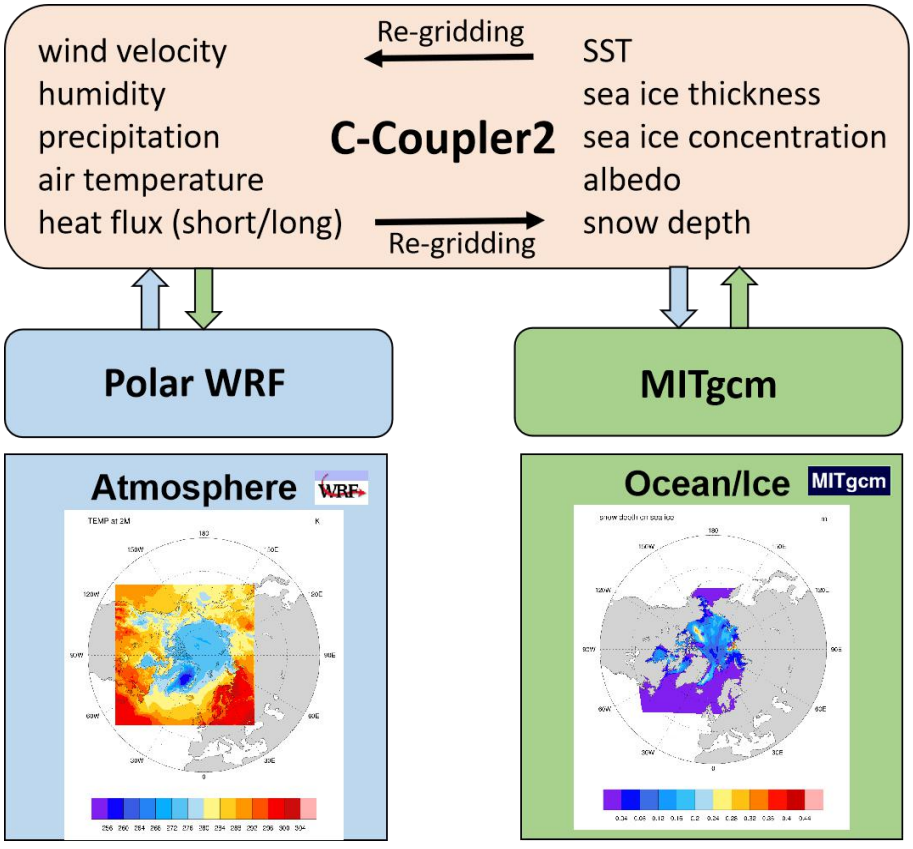

Figure 1: Coupling strategy of the Polar WRF-MITgcm coupled model system.

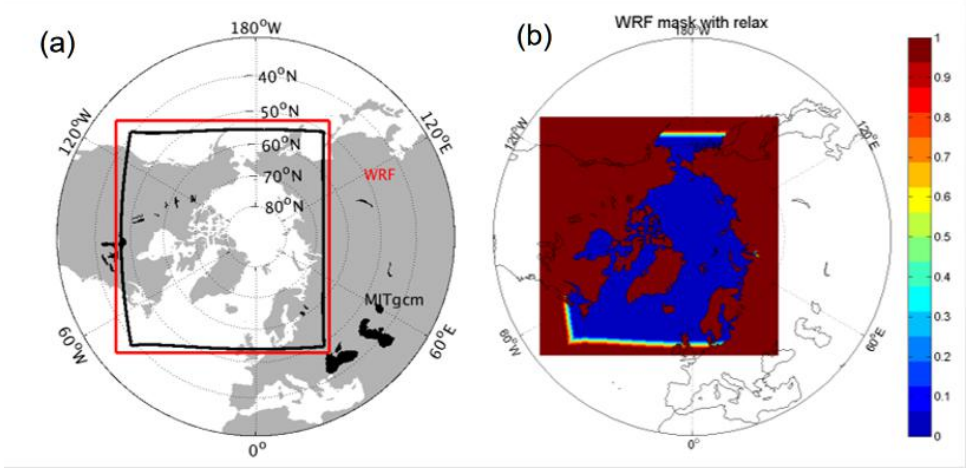

Figure 2: (a) Model domain of the MITgcm and the Polar WRF model. The red and black lines denote the boundaries of the Polar WRF and the MITgcm model, respectively. (b) Relaxation coefficient for the external forcing file of the Polar WRF bottom boundary conditions.

https://doi.org/10.5194/gmd-2020-95
Preprint. Discussion started: 19 June 2020

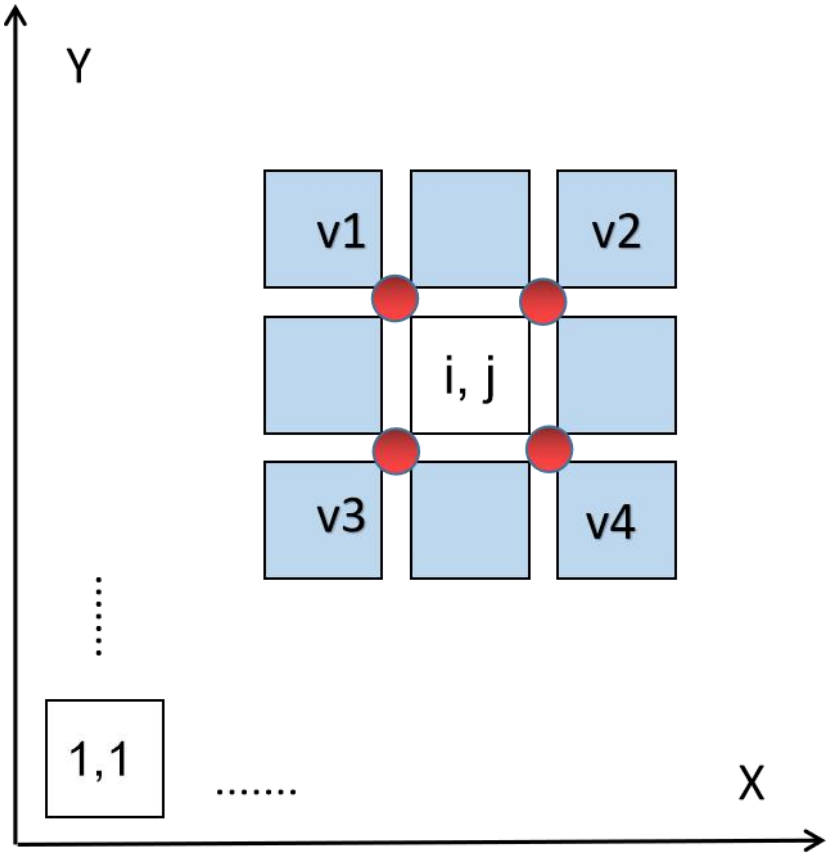

595 **Figure 3: Schematic diagram of calculating the corner geographic information of the MITgcm grid.**

https://doi.org/10.5194/gmd-2020-95
Preprint. Discussion started: 19 June 2020

Geoscientific Model Development Discussions

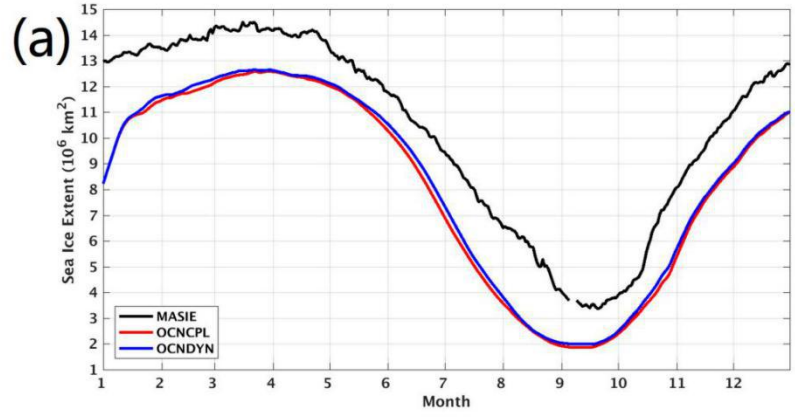

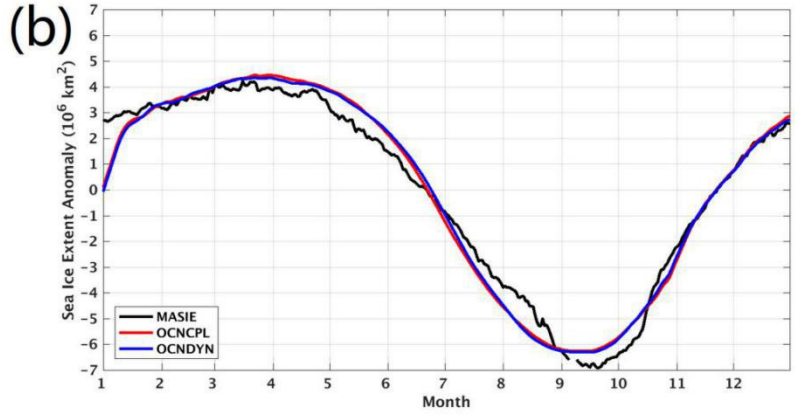

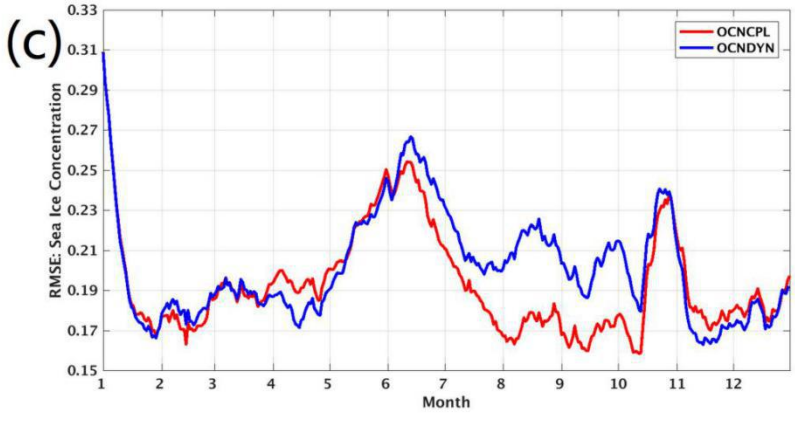

Figure 4: Time series of (a) sea ice extent, (b) sea ice extent anomaly, and (c) root mean square error (RMSE) of modeled sea ice concentration with respect to the OSISAF observation in 2012. The black, red, and blue lines in (a) denote sea ice extent of the MASIE observation, the OCNCPL run, and the OCNDYN run, respectively. The black, red, and blue lines in (b) denote sea ice extent anomaly of the MASIE observation, the OCNCPL run, and the OCNDYN run, respectively. The red and blue lines in (c) denote the sea ice concentration RMSE of the OCNCPL run and the OCNDYN run, respectively. MASIE = Multisensor Analyzed Sea Ice Extent; OSISAF = Ocean and Sea Ice Satellite Application Facility.

https://doi.org/10.5194/gmd-2020-95
Preprint. Discussion started: 19 June 2020

Geoscientific Model Development Discussions

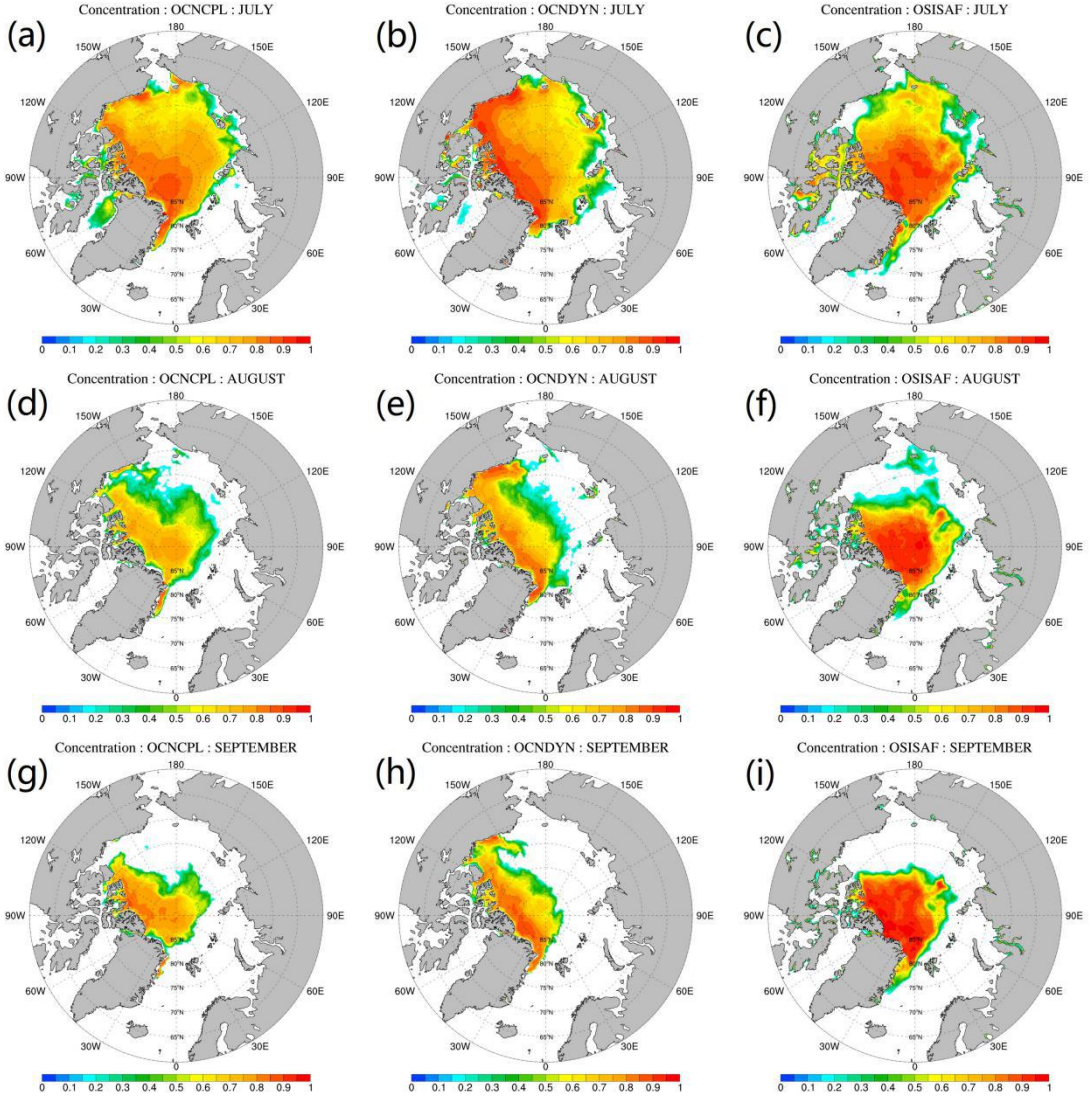

Figure 5: Modeled and observed monthly mean sea ice concentration. The top, middle, and bottom panels show the July, August, and September sea ice concentration, respectively. The left, middle, and right panels show sea ice concentration of the OCNCPL run, the OCNDYN run, and the OSISAF observations. OSISAF = Ocean and Sea Ice Satellite Application Facility.

https://doi.org/10.5194/gmd-2020-95
Preprint. Discussion started: 19 June 2020

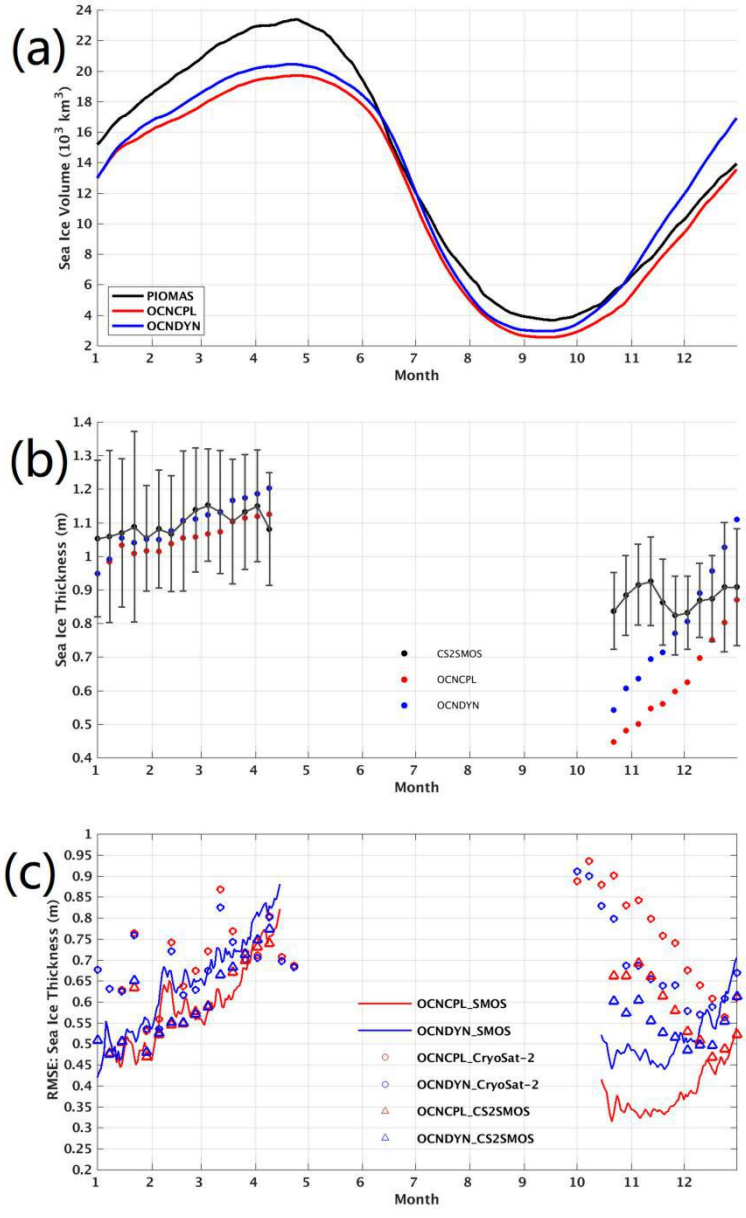

Figure 6: Time series of (a) total sea ice volume, (b) spatial mean sea ice thickness, and (c) the RMSE of sea ice thickness with respect to the satellite-retrieved observations in 2012. The black, red, and blue lines in (a) denote total sea ice volume of the PIOMAS data, the OCNCPL run, and the OCNDYN run, respectively. The black, red, and blue dots in (b) denote sea ice thickness of the CS2SMOS observations, the OCNCPL run, and the OCNDYN run, respectively. The black bar in (b) represents the observational uncertainties of the CS2SMOS data. The red and blue masks in (c) denote sea ice thickness RMSE of the OCNCPL run and the OCNDYN run with respect to the SMOS observations in thin ice (< 1 m) region (line), the Cryosat-2 observations (circle), the CS2SMOS observations (triangle), respectively. Model grid points without available observations are not taken into the sea ice thickness RMSE calculation. PIOMAS = Pan-Arctic Ice Ocean Modeling and Assimilation System; SMOS = Soil Moisture Ocean Salinity.

https://doi.org/10.5194/gmd-2020-95
Preprint. Discussion started: 19 June 2020

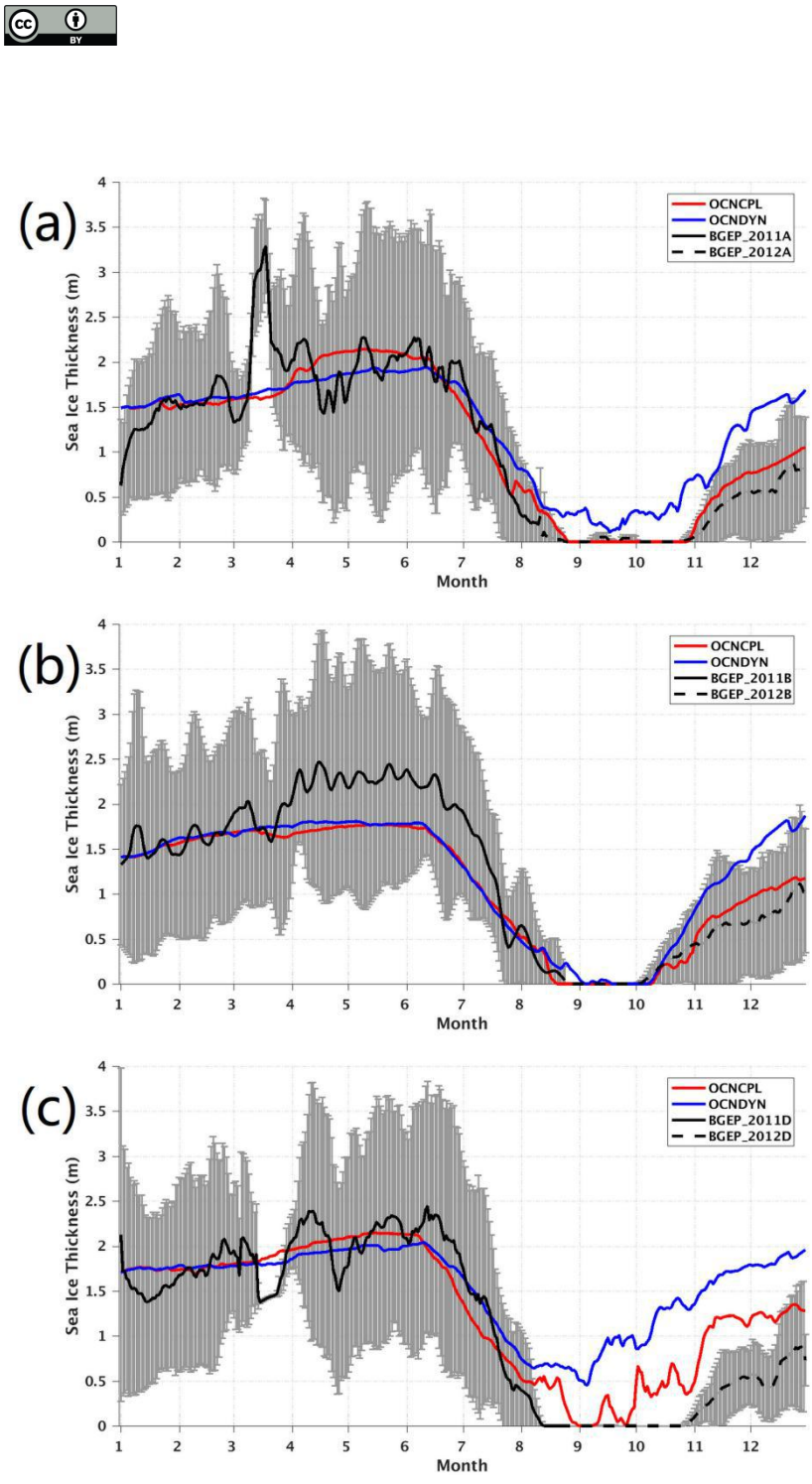

Figure 7: Time series of sea ice thickness at three positions: (a) (75 °N, 150 °W), (b) (78 °N, 150 °W), and (c) (74 °N, 140 °W). The red and blue lines denote sea ice thickness of the OCNCPL run and the OCNDYN run, respectively. The black solid and dashed lines denote sea ice thickness observations of the BGEP ULSs, which were deployed in the summers of 2011 and 2012. The black lines of the BGEP ULS observations have been smoothed with the gray bar representing the observational uncertainties. BGEP = Beaufort Gyre Exploration Project; ULS = upward-looking sonar.

https://doi.org/10.5194/gmd-2020-95
Preprint. Discussion started: 19 June 2020

Geoscientific Model Development Discussions
Open Access
EGU

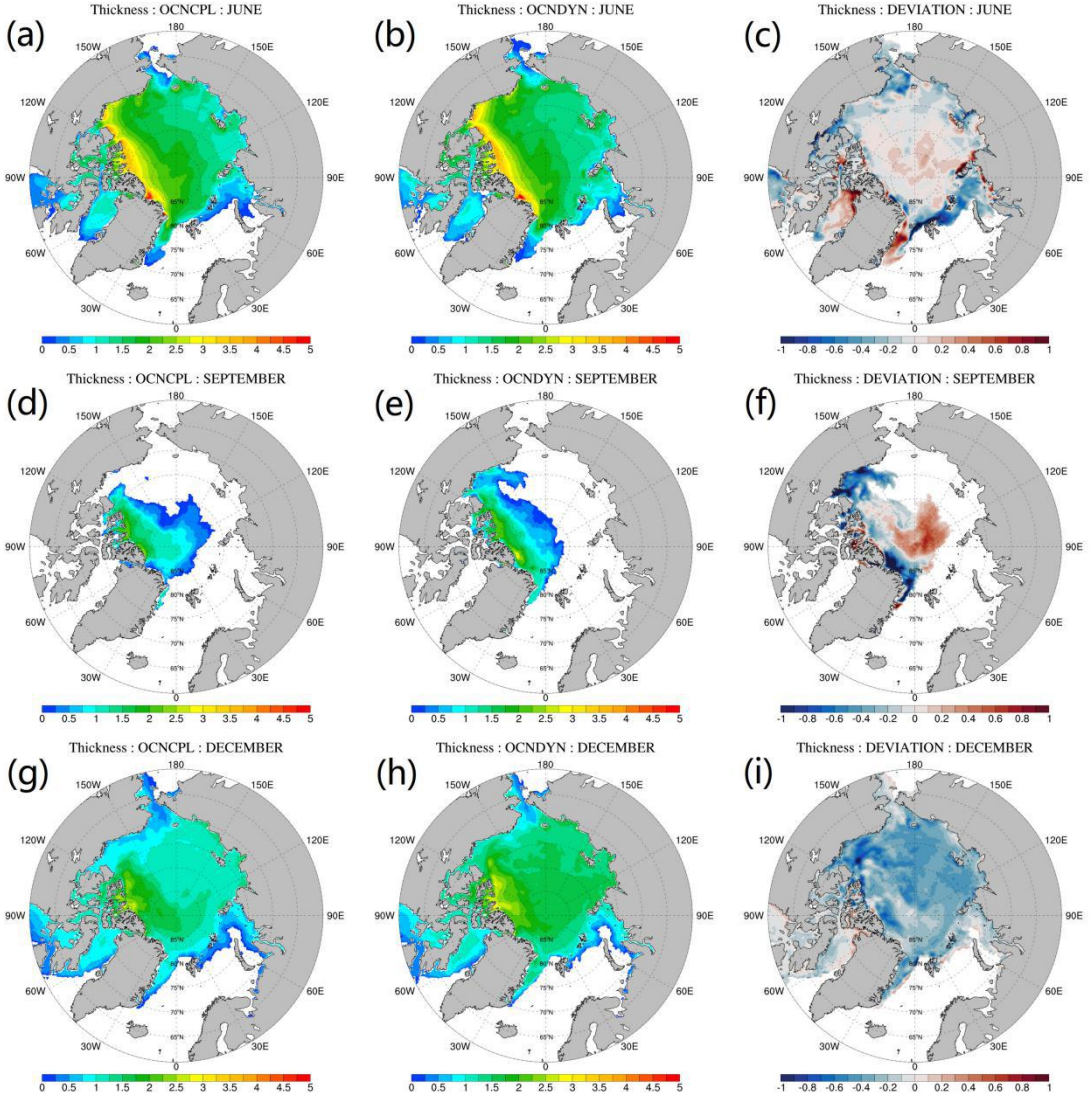

Figure 8: Monthly mean sea ice thickness. The top, middle, and bottom panels show the June, September, and December sea ice thickness, respectively. The left, middle, and right panels show sea ice thickness of the OCNCPL run, the OCNDYN run, and the deviation between them.

https://doi.org/10.5194/gmd-2020-95
Preprint. Discussion started: 19 June 2020

Geoscientific Model Development Discussions
Open Access
EGU

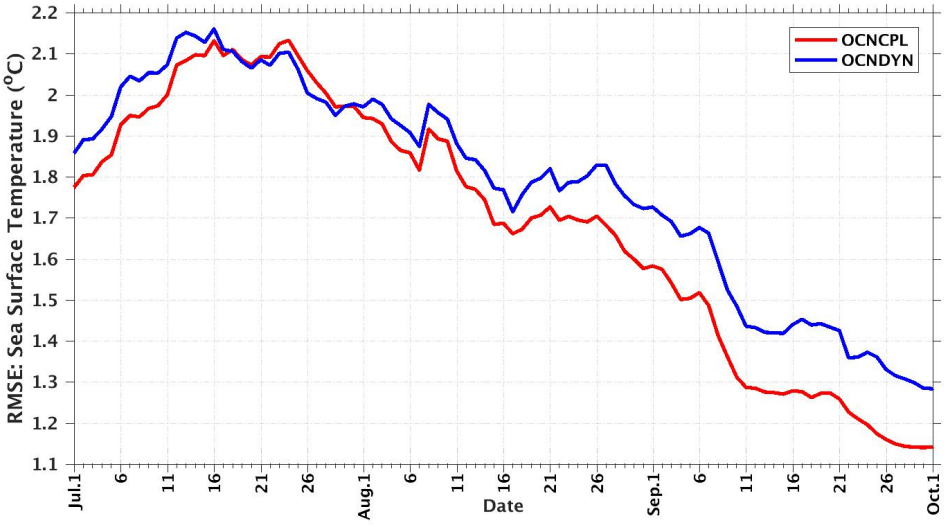

Figure 9: Time series of the RMSE of modeled SST with respect to the GMPE observations in summer of 2012. The red and blue lines denote the SST RMSE of the OCNCPL run and the OCNDYN run, respectively. GMPE = Group for High-Resolution Sea Surface Temperature Multi-Product Ensemble.

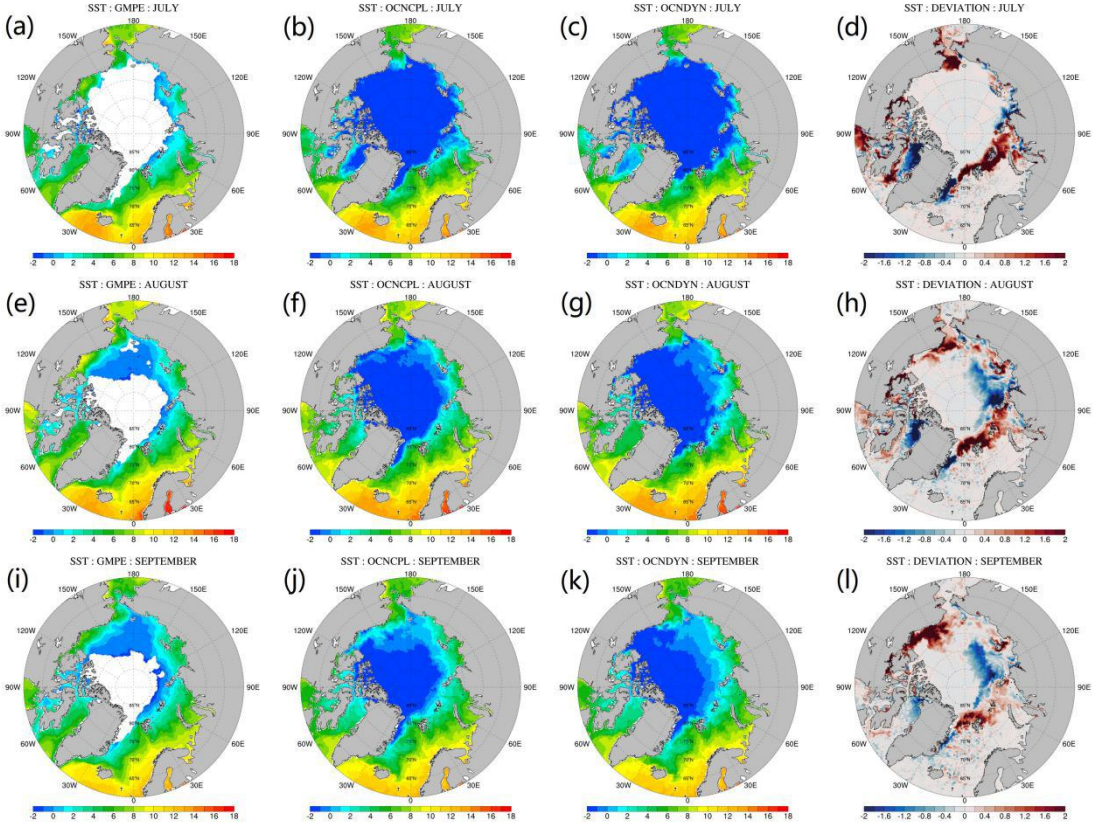

https://doi.org/10.5194/gmd-2020-95
Preprint. Discussion started: 19 June 2020

Geoscientific Model Development Discussions

Figure 10: Modeled and observed monthly mean SST. Rows 1 to 3 show the July, August, and September SST, respectively. Columns 1 to 4 show the SST of the GMPE observations, the OCNCPL run, the OCNDYN run, and the deviation between the OCNCPL and OCNDYN runs, respectively. GMPE = Group for High-Resolution Sea Surface Temperature Multi-Product Ensemble.

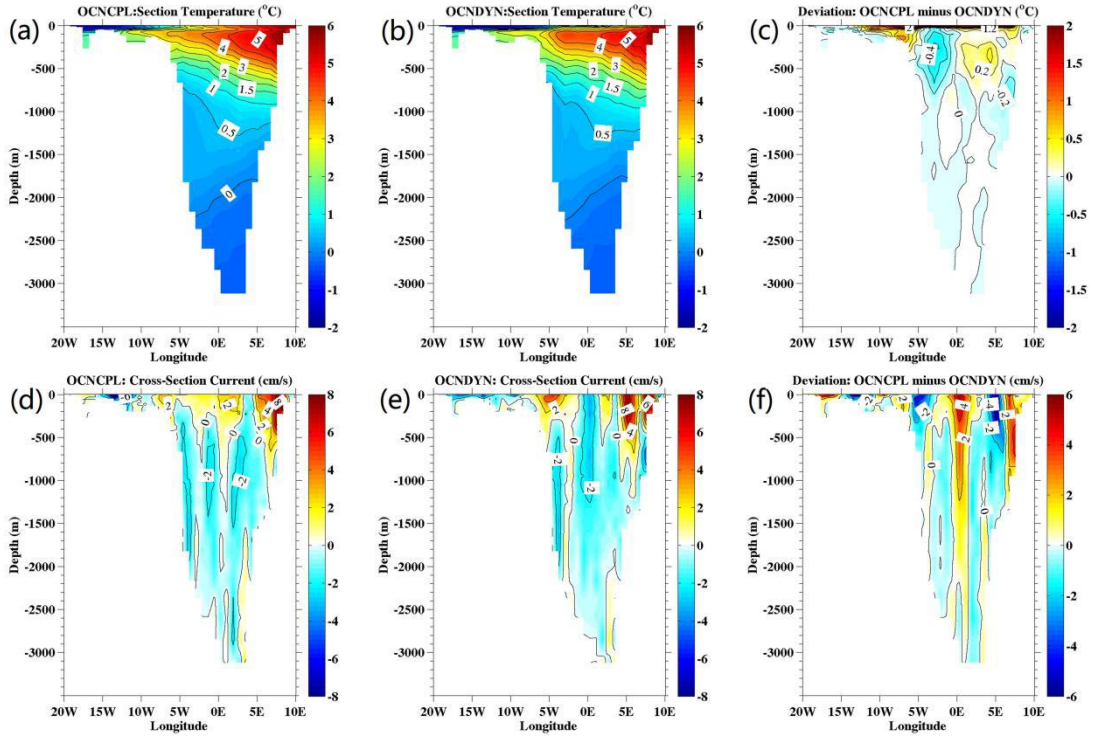

Figure 11: July-August-September mean ocean temperature and meridional velocity section along 78 °N in Fram Strait. The top and bottom panels show the ocean temperature and meridional velocity, respectively. The left, middle, and right panels show the OCNCPL run, the OCNDYN run, and the deviation between them, respectively.

https://doi.org/10.5194/gmd-2020-95
Preprint. Discussion started: 19 June 2020

Geoscientific Model Development Discussions

Table 1: Monthly mean northward cross-section velocity (cm/s) and temperature (°C) averaged between 5°E and 8°40'E at 78°50'N in Fram Strait. A1 represents algorithm 1 that values are calculated from sea water with potential temperature higher than 1°C. A2 represents algorithm 2 that values are calculated from sea water with potential temperature higher than -0.1°C. A3 represents algorithm 3 that values are calculated from sea water with depth shallower than 700 m. The observations are averaged between 1998 and 2003. WSCOBS = West Spitsbergen Current Observation.

		July		August		September	
		V_{mean}	T_{mean}	V_{mean}	T_{mean}	V_{mean}	T_{mean}
A1: (T>1°C)	OCNCPL	3.94	3.56	4.03	3.66	4.03	4.02
	OCNDYN	3.22	3.69	2.93	3.79	2.27	3.91
	WSCOBS	6.26	2.76	6.98	2.90	7.36	3.02
A2: (T>-0.1°C)	OCNCPL	3.53	2.30	3.32	2.35	3.24	2.54
	OCNDYN	2.63	2.58	2.38	2.69	1.98	2.66
	WSCOBS	5.82	2.35	6.39	2.44	6.69	2.51
A3: (0-700 m)	OCNCPL	4.21	3.97	4.33	4.03	4.16	4.53
	OCNDYN	3.87	4.36	3.53	4.54	2.55	4.65
	WSCOBS	6.09	2.61	6.67	2.72	7.04	2.83